Metals & corrosion

The heterogeneous nature of mechanically accelerated grain growth

Elton Y. Chen[1], Parker Hamilton[1,2], Brad L. Boyce[1], and Rémi Dingreville[1,*]

[1] *Center for Integrated Nanotechnologies, Sandia National Laboratories, Albuquerque, NM 87185, USA*
[2] *Brigham Young University, Provo, UT 84602, USA*

ABSTRACT

While grain growth is traditionally viewed as a purely thermally driven process, nanocrystalline metals can undergo grain growth under mechanical loads, even at room temperature. We performed a detailed atomistic study of the heterogeneous nature of mechanically accelerated grain growth in a polycrystalline Pt nanowire. Using molecular dynamics simulations, we compared the grain-growth behavior of individual grains during tensile and shear cyclic loading, for three different equivalent strain levels, and at two temperatures. Pure thermal grain growth with no mechanical loading provided a baseline reference case. On average, grains that were already susceptible to thermal grain growth were stimulated to grow faster with mechanical loading, as expected. However, when analyzed on a grain-by-grain basis, the results were far more complex: grains that grew fastest under one stimuli were less accelerated under other stimuli. Even when the magnitude of loading changed, the relative growth of individual grains was distorted. We interpret this complexity from the perspective of superimposed growth mechanisms.

Introduction

Mechanically assisted grain growth is a microstructural instability mechanism that has been recognized for decades [1–4] and which consists of the coarsening of a grain structure caused by, or accelerated by, mechanical stresses or strains. While grain growth is traditionally viewed as a purely thermal process that requires elevated temperatures, some metals can undergo grain growth even at room temperature or below due to mechanical loading. This mechanism is commonly reported in a broad range of nanocrystalline metals, for uniaxial [5–8], high-pressure torsion [9, 10], indentation [11, 12], or cyclic loading [13–19], at both room and cryogenic temperatures [20–23]. For instance, Gianola et al. [5] reported accelerated, discontinuous room temperature grain

Springer

growth in nanocrystalline aluminum (Al) as a direct result of the applied deformation. Similarly, Liao and coworkers [9] studied grain growth in electrodeposited nanocrystalline nickel (Ni) during high-pressure torsion and revealed that the upper limit of grain size is determined by the deformation mode. For some material systems, only certain loading conditions result in mechanically assisted grain growth. Nanocrystalline platinum (Pt) exhibits this peculiarity. Meirom and coworkers [14] observed that nanocrystalline Pt thin films tested under cyclic loading showed grain growth but films tested under tensile loading did not. However, Sharon et al. [8] noticed grain growth in nanocrystalline Pt due to tensile loading. The differences between the two studies suggest that depending on the microstructure (columnar, textured microstructure in the Meirom case vs. random, equiaxed microstructure for Sharon), only certain mechanical loading paths provide enough driving force to cause coarsening. Taken together, these different studies point to the role of the local stress and strain fields on grain-boundary motion and the existence of different mechanisms of grain-boundary motion leading to mechanically accelerated grain growth in nanocrystalline materials. In all cases, these observations illustrate that grain growth only occurs under particular deformation modes and for particular distribution of local stress and deformation fields. The study by Rupert et al. [7] is a prime example of this assertion. They used freestanding nanocrystalline Al thin films with specific geometries to separate the relative importance of normal vs. shear stresses and demonstrated that the grain growth observed in those thin films was associated with grain-boundary migration driven by shear stresses.

The couplings and correlations between mechanical loads, grain-boundary migration, and grain growth have been studied for bi-crystals and nanocrystalline configurations via numerous atomistic and mesoscale simulations. For the most part, bi-crystal simulations focused on idealized, planar grain-boundary configurations [24–34] and described possible unit mechanisms associated with mechanically driven grain-boundary motion, or they provided energetic and kinematic properties of boundaries as a function of their attributes such as grain-boundary energy or structural characteristics. For instance, Trautt and coworkers [29] investigated the stress-driven motion of asymmetrical grain

boundaries as a function of inclination angles in copper (Cu) and Al. Their results showed the existence of multiple coupling modes for different grain-boundary inclination angles. Aramfard and Deng [33] compared the effects between constant loading and cyclic tensile/compressive loading on the motion of two high-angle symmetric grain boundaries. They found that in both cases these boundaries experienced a structural phase transformation upon mechanical loading and that this structural change is larger in the case of cyclic loading as compared to the monotonic loading. Omlsted et al. [26] surveyed the mobility of 388 different boundary configurations and discovered that mobility is not always thermally activated. Complementing the idealized, planar, bi-crystal studies, simulations focused on polycrystalline systems [35–43] provided insights into the cooperative role that grain-boundary network and various active mechanisms play on mechanically assisted grain growth. For example, Panzarino et al. [42] measured the relative contributions of grain rotation and grain-boundary sliding on grain coarsening in nanocrystalline Al during cycling loading using molecular dynamic simulations. Similarly, Foiles et al. [43] performed static and cyclic loading atomistic simulations on a nanocrystalline Ni nanowire at both 300 and 500 K and compared the effect of both deformation mode and temperature on the average grain-growth behavior.

The experimental and simulation examples above suggest that there is a variety of different mechanisms which can contribute to mechanically assisted grain growth. As a result, we anticipate that different grains and grain boundaries may respond heterogeneously under a variety of stimuli. That that end, we used molecular dynamics simulations to study the grain structure evolution in a nanocrystalline Pt nanowire subjected to various thermal and cyclic loading conditions. We specifically focus on low cycle tensile and shear loading conditions since they can exacerbate grain growth as opposed to monotonic loading. We chose Pt since it is a material system that has showed sensitivity to only certain loading conditions. During cycling for two deformation modes, at three different strain levels, and at two temperatures, we compare and contrast the growth behavior of multiple grains that dominate the overall grain-boundary network behavior. These mechanisms and individual grain-growth behavior are found to be non-uniform across grains and dependent on the

deformation mode and temperature, leading to complex reorganization of the grain structure with multiplicative effects.

Methods

We carried out our atomistic simulations using the open-source molecular dynamics code large-scale atomic/molecular massively parallel simulator (LAMMPS) [44]. These simulations consisted of constructing a nanocrystalline Pt nanowire with an initial grain microstructure physically realistic and then subjecting it to different types of cyclic loading at various temperatures. We observed and quantified the evolution of the grain structure of the wire for thermal annealing and tensile and shear cyclic conditions using the Open Visualization Tool (OVITO) [45].

Interatomic potential and microstructure

We modeled the grain structure evolution in a nanocrystalline Pt nanowire. In addition to being sensitive to loading conditions, we selected Pt as a model material system due to its favorable face-centered-cubic (FCC) crystal structure and high melting temperature, which lessens the effect of thermal creep during cyclic loading. We used an interatomic potential of the embedded atom method form parameterized by Sheng [46] to describe the atomic interactions in Pt. Based on the data used to fit this potential, it provides a suitable description of phonon behaviors, thermal properties, and stacking-fault and grain-boundary energies, all of which are important properties for grain growth.

Utilizing the earlier synthetic nanowire microstructure of Foiles et al. [43], we adapted this realistic microstructure to Pt from the original FCC Ni system. The motivation for using such realistic microstructure is based on previous studies [47, 48] which showed that the details of the evolution of microstructure during mechanical deformation is sensitive to the details of the initial atomic structure employed. The Ni nanowire microstructure was first converted to Pt by scaling the atomic positions from the ratio of lattice constants and minimizing the energy of the entire nanowire at 0 K using the appropriate interatomic potential. We then relaxed the nanocrystalline Pt nanowire to an ambient

temperature of 300 K over 200 ps, where the temperature was maintained using a Langevin thermostat [49]. As illustrated in Fig. 1a, the initial nanowire configuration is composed of a total of 3,348,856 atoms. The simulation cell is periodic along the main axis of the nanowire (Z-direction) in order to emulate an infinitely long wire. A zero-pressure boundary condition was applied in the Z-direction during thermal relaxation to remove any excess stress that may have araised when switching the lattice from Ni to Pt. The final relaxed Pt nanowire configuration is approximately 40 × 40 × 46 nm in dimension, with initially 555 grains. Initial dimensions of the wire were subsequently used to determine the strain-controlled mechanical loading.

Grain growth simulations

To induce grain growth in a time frame observable in a molecular-dynamics setting, we used a combination of both thermal annealing and cyclic mechanical loading. For the annealing simulations, similar to the initial relaxation step described above, the baseline thermal anneal was conducted using a Langevin thermostat with a zero-pressure condition enforced in the periodic Z-direction. In these simulations, the nanowire was relaxed for a period of 5 ns over 5,000,000 time steps to simulate the process of steady state grain growth. We tested annealing temperatures of 400, 600, and 800 K. However, we ultimately ignored the results at 800 K since at this temperature the thermal-dominant grain growth mechanism would overshadow the effects of any applied mechanical loading.

For the application of mechanical loads, we simulated the Pt nanowire mechanically loaded with both tensile and shear cyclic loads, respectively. Regarding the tensile cyclic loading simulations, at 400 and 600 K, we applied strain-controlled, tensile back-to-neutral loads to the wire by stretching and relaxing the nanowire in the periodic Z-direction. Each tension cycle occurred over a period of 100 ps, for 50 cycles over the total 5 ns simulation time (i.e., corresponding to a frequency of 10 GHz). We tested tensile strains ϵ_{zz} with magnitudes of 0.6, 0.8, and 1.0% to match those typically applied during experiments. We show in Fig. 1c a representative stress and displacement observed during the ϵ_{zz} = 1.0% cyclic loading. The shear cyclic loading simulations were similar to that of the tensile case. The simulation cell
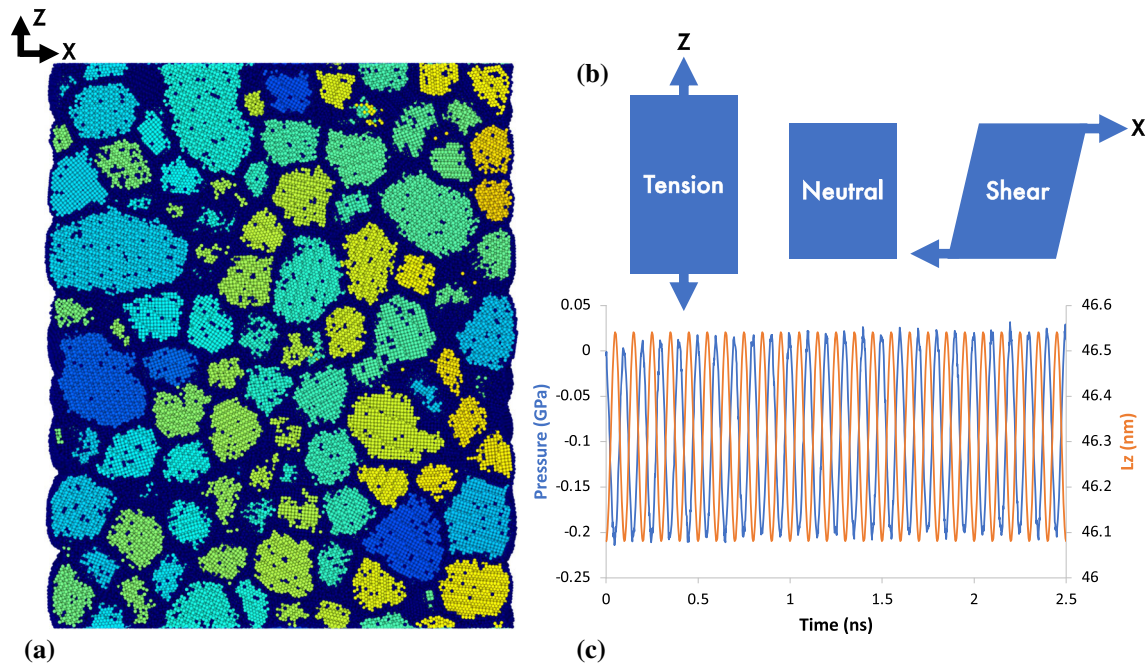
Figure 1 *Atomistic simulation setup.* **a** Initial nanowire model obtained from Foiles et al. [43]. The nanowire configuration was converted from Ni to Pt. **b** Schematics of cyclic loading. **c** Variation of the stress and displacement of the nanowire during cyclic loading. As an example, this plot reflects the tensile cyclic loading with a strain ϵ_{zz} of 1.0% for the first 2.5 ns. Color coding in **a** is used to differentiate grains..

was first converted to triclinic and then cyclically tilted in the XZ direction as shown in the schematic of Fig. 1b. To achieve some degrees of comparison between the two modes of deformation, we imposed shear strains ϵ_{ij} calculated using equivalent von Mises strain conditions: $\epsilon_{eq} = \frac{2}{3}\sqrt{\frac{3(e_{xx}^2+e_{yy}^2+e_{zz}^2)}{2}+\frac{3(\gamma_{xy}^2+\gamma_{yz}^2+\gamma_{zx}^2)}{4}}$, where $e_{xx} = +\frac{2}{3}\epsilon_{xx} - \frac{1}{3}\epsilon_{yy} + \frac{1}{3}\epsilon_{zz}$ are deviatoric strains and $\gamma_{ij} = 2\epsilon_{ij}$ are the engineering shear strains. For each shear strain load, the von Mises equivalent strain conversion approximates to a factor of 1.1547. Note that the cycle rate is the same between tensile and shear cyclic loads. Initially, we also considered near cryogenic temperature isotherm mechanical loading. However, scoping tests confirmed that without the necessary thermal mobility, these low mechanical loads alone were not sufficient to produce notable grain growth within the molecular dynamics time frame.

Grain statistics

For the extraction of grain-growth statistics, we used a combination of polyhedral template matching and nearest-neighbor analysis [50, 51]. Through this process we could identify and eliminate the disordered boundary atoms from contention. Orientation was

then computed for each remaining crystalline atom. Finally, we used a burn algorithm to identify the contiguous grains with atoms of similar orientation. Each grain was identified by its initial size, with a grain identity (GID) of 1 being assigned to the largest grain and so on. We finally used a time progression mass-centroid analysis for each output time frame to track the individual grain dynamics and the grain growth/shrinkage behavior. The size of each individual grain was calculated as the number of atoms within specific grain multiplied by the atomic volume. The grain size was calculated as the diameter of a three-dimensional sphere with equivalent volume as the grain being investigated.

Results

Grain-growth behavior under baseline thermal annealing conditions

Since it is difficult to separate the thermally activated part of grain growth from its mechanically assisted part in the simulations, it is important to first establish a baseline behavior of grain growth during simple thermal anneals. Hence, we first simulated grain growth at elevated temperatures of 400, 600 and 800
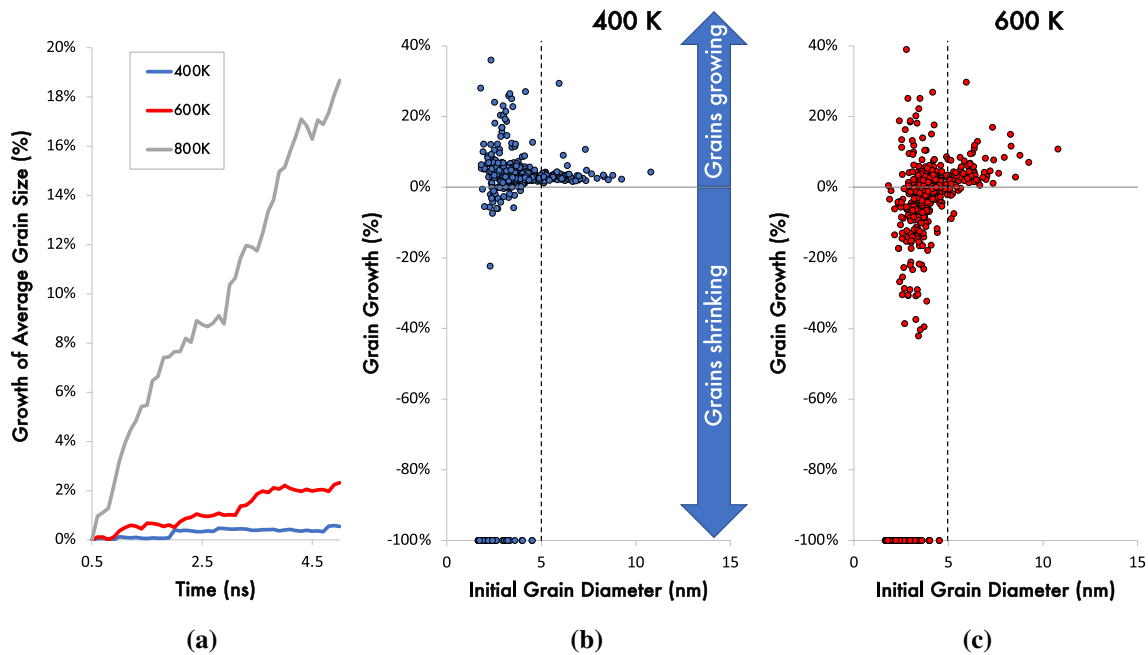
Figure 2 *Average grain growth in the nanowire.* **a** Growth of the average grain size at different annealing temperatures. Results from the 800 K anneal are considered too thermally driven, therefore not included in subsequent combined mechanical loading analyses. **b, c** Distribution of grain-growth behavior as a function of the initial size of the grains at 400 and 600 K, respectively.

K over 5 ns, without any mechanical loading. Figure 2a illustrates the resultant average grain growth at these three respective temperatures. Here the evaluation of the grain-growth behavior was conducted using the change in average grain size over the entire nanowire. We truncated the first 0.5 ns to eliminate any transient loading behavior and performed our analysis during the steady-state grain-growth regime. We adopted this procedure in the remainder of the result section. First, we note that across all the temperatures tested, the average grain size grows as a linear function of annealing time. After 5 ns, the final average grain growths are 1.0, 2.0, and 19.0% at 400, 600, and 800 K, respectively. Due to the extremely rapid thermal grain growth at 800 K, we deemed the 800 K baseline unsuitable for any additional mechanical load testing since thermal effects would dominate the grain-growth behavior.

The scatter plots in panels (b) and (c) of Fig. 2 show how the average grain growth is distributed across the various grains as a function of their initial individual grain diameters at both annealing temperatures of 400 and 600 K, respectively. We note that there is a greater portion of grains that shrink at the higher temperature of 600 K as compared to 400 K, with the addition of 95 grains ($\sim 17\%$) that have been completely consumed at 600 K and slightly less than half of that number at 400 K with 46 grains ($\sim 8\%$).

This trend is expected given the greater contribution of thermally assisted grain growth with increasing temperature. At 600 K, grains bigger than 5 nm in diameter would always grow, while at 400 K this threshold happens for grains bigger than 6 nm. Finally, we also note that there is a substantial fraction of small grains that grew. Collectively, these scatter plots illustrate the non-uniform growth behavior of individual grains within the nanocrystalline system.

Disparity of growth behaviors under mechanical loads

The results in Fig. 3a, b are focused on the grain-growth behavior of the initially largest grain (GID = 1) as it is the center of attention in classical abnormal grain-growth analyses [43]. We compare the growth behaviors of grain GID = 1 when the nanowire is cyclically loaded in tension and shear at various strain levels (from 0.6 to 1.0% strain level) and at two temperatures of 400 K (a) and 600 K (b), respectively. It is important to note that since grain growth is heterogeneous within the nanowire, growth of individual grains can outpace or dawdle the average grain growth averaged over the entire microstructure. Indeed, for grain GID = 1, its grain growth is over 7% at 400 K (as compared to an average growth
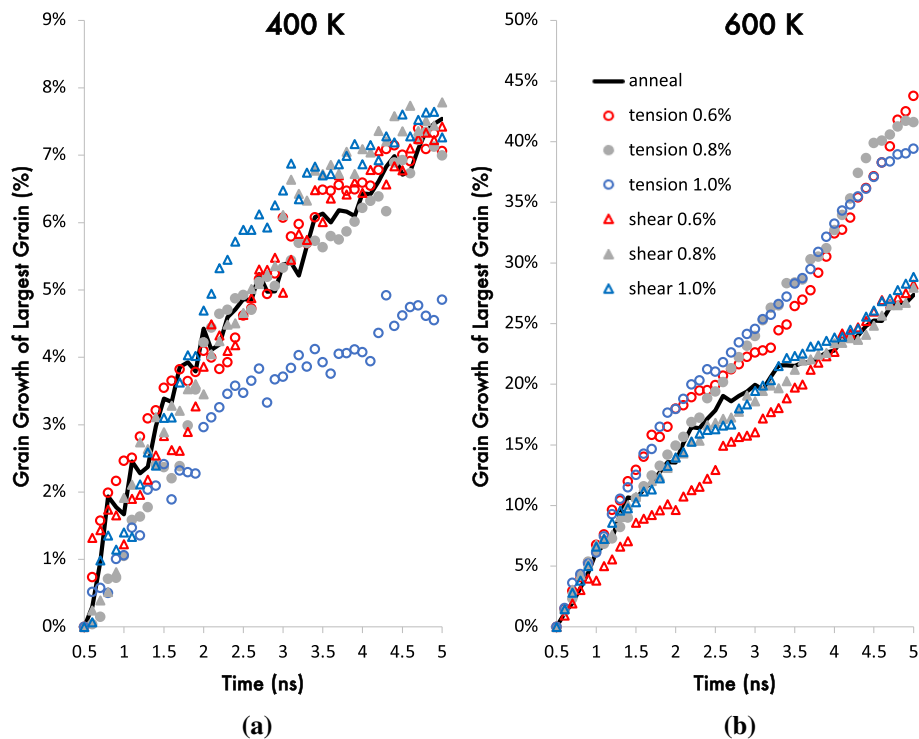
Figure 3 *Growth behavior of largest grain*. **a** Growth of the initially largest grain (GID = 1) at 400 K. The superposition of the six different mechanical loading conditions modified the grain growth trajectory above or below the baseline annealing case. Surprisingly, the 1% tensile strain case suppressed grain growth. **b** Growth of GID = 1 at 600 K. With respect to the current strain rate, tensile cyclic loading presents significant acceleration of the

grain growth as compared to shear cyclic loading and from baseline anneal. No clear differentiation between the different loading magnitudes is observed. Circular symbols indicate results for tensile cyclic loading, triangular symbols indicate results for shear cyclic loading, and the thick black line represents results for the baseline thermal anneal.

rate of 2.47% averaged over all the grains) and 40% at 600 K (as compared to an average growth rate of 12.56% averaged over all the grains). When comparing the relative grain growth at 400 K, the additional mechanical loads do not have any notable effect on grain GID = 1, with only the 1% tensile strain cyclic case as the outlier (4% relative growth as compared to $\sim$ 7.5% relative growth in all the other cases). At 600 K, the different mechanical loading modes can be differentiated from one another. At this temperature, the tensile cyclic loading accelerated the growth of the initially largest grain regardless of the strain level applied. While, for the shear cases, the grain-growth behavior seems to be similar to the simple thermal anneal baseline case. While not shown in this figure, this change in grain-growth behavior as a function of the mode of mechanical loading was a common trend observed across many large grains.

As we expand the analysis beyond the largest single grain, a more complex taxonomy of differential grain-growth behaviors emerge. In order to extract

the differential effects of the mechanical cyclic loading and compare multiple grains, we have expanded the results from Figs. 2 to 3 by comparing the grain growth rates (GGR) under different loading conditions for the ten largest grains at the end of simulation in Fig. 4. The GGR, a_{GGR}, was measured by fitting the growth of individual grains with the functional form $y_{gs} = a_{GGR} \ln(\Delta t) + y_0$, where y_{gs} is the grain size, Δt is the time step, and y_0 is the initial grain size. Note that grain GID = 10 is not included in this analysis, as it was consistently outgrown by grain GID = 11 after 5 ns of simulation time. Comparing the two temperatures (400 K in (a) and 600 K in (b)), we can easily observe that the GGRs are significantly accelerated at 600 K as compared to those at 400 K. Interestingly, while grain GID = 1 is by far the largest grain pre- and post-growth, it is not always the fastest growing grain. Instead, grain GID = 6 is the *de facto* fastest growing grain at 600 K under all loading conditions. Similarly, grain GID = 11 exhibited exceptional GGRs at 600 K not found at 400 K. These trends indicate that

Figure 4 *Grain growth rate for the 10 final largest grains at* **a** *400 K and* **b** *600 K. Grains remain consistent regardless of thermal and mechanical loads. Grain growth rate a_{GGR} as fitted to function* $y_{gs} = a_{GGR} \ln(\Delta t) + y_0$. *Positive grain growths are present in almost all conditions. While growth is noticeably higher at 600 K than 400 K, the fastest growing grain changes from grain GID = 1 at 400 K to grain GID = 6 at 600 K.*
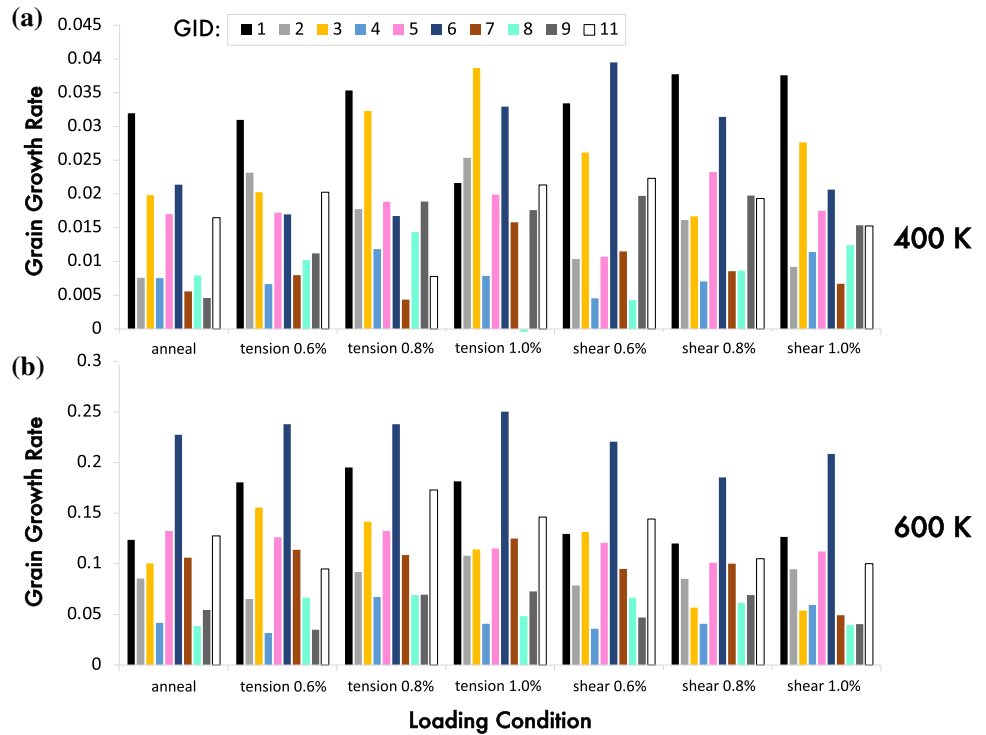
GGRs are not only independent of grain size, but also preferentially vary with temperature.

We further calculated the change in GGRs, ΔGGR, with respect to the baseline anneal in Fig. 5. This relative change is calculated as $\Delta GGR = (a_{GGR} - a_{anneal})/a_{anneal}$, where a_{anneal} is the GGR for simple thermal anneal. This figure reveals that the mechanical effects are more prominent at the less thermally dominant 400 K than at 600 K. Particularly at 400 K, the two grains of interest are grains GID = 2 and GID = 9. Both of these grains exhibited large GGR acceleration with the addition of mechanical cyclic loading. For grain GID = 2, these accelerations appear to be primarily correlated with the application of tensile cyclic loading, with only 0.8% strain shear cyclic loading demonstrating notable change. For grain GID = 9, the GGRs are consistently affected by the presence of mechanical load, regardless of the deformation mode.

At the higher temperature of 600 K, the relative changes in GGRs are less prominent as the grain growth becomes more thermally driven. Under such temperature condition, grain GID = 8 becomes the only grain that is consistently experiencing an accelerated growth by the addition of mechanical cyclic loading. Although less apparent, but more important, is the trend of negative change/deceleration of GGRs across the shear cyclic loading cases. This trend

indicates that the application of mechanical loads may not be universally beneficial to grain growth. Rather, it could be detrimental depending on the combination of grain and loading mode. In fact, the examination of Fig. 5 in detail reveals that grain GID = 7 is always negatively affected by shear cyclic loading for all strain magnitudes.

Disparity in growth mechanisms

The results in the previous section illustrated the variability in growth behavior of individual grains, but they did not provide insights into the underlying growth mechanisms. To illustrate the complexity and heterogeneous nature of the grain-growth behavior described above, all ten grains of interest are rendered in Fig. 6. These grains are mostly spatially isolated within the nanowire, suggesting a lack of direct competition between one another. Conventional theory states that grain growth should scale with the size of a grain [52, 53]. However, comparison of grains GID = 1 and GID = 6 reveal that this is not necessarily the case. Indeed, as shown in the render of grain GID = 6, we observe a much accelerated growth after 5 ns of thermal anneal at the same temperature of 600 K. The highly mechanically accelerated grains GID = 2 and 9 at 400 K are also shown in this figure. These grains however lack any abnormal geometrical changes with the application of

Figure 5 *Change in grain growth rate (GGR) relative to anneal induced by cyclic loading at* **a** *400 K and* **b** *600 K. Grain growth rates are impacted differently by mechanical loading conditions. Grains GID = 2 and GID = 9 are most affected by cyclic loading at 400 K. Grain GID = 5 is negatively affected by both tensile and shear cyclic loads at 600 K; grain GID=7 is negatively affected by shear cyclic loading at 600 K.*
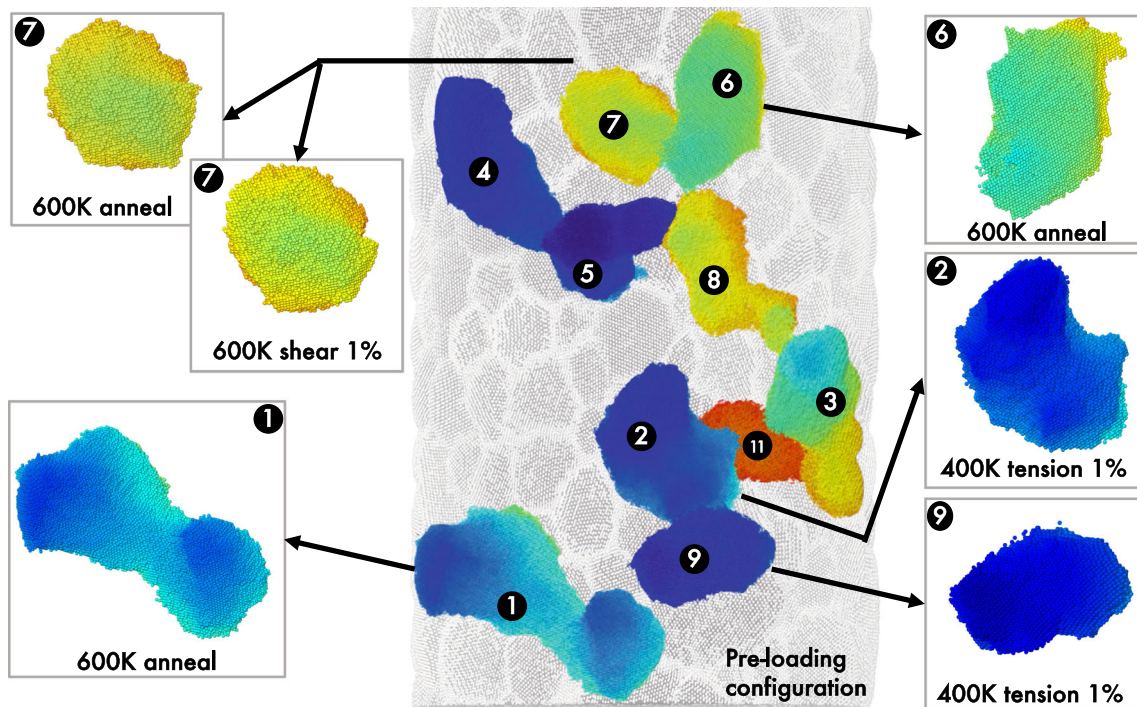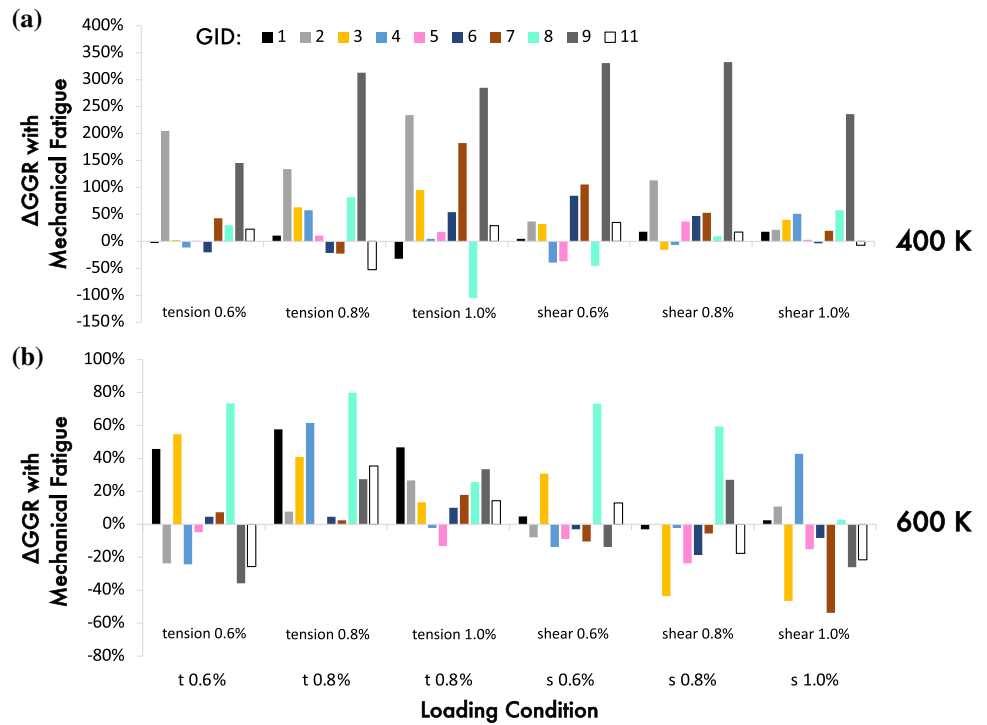

Figure 6 *Spatial distribution of the ten largest grains at the end of the simulation.* These ten largest grains are largely independent with no significant common boundaries between them. Extraordinary growth cases for grains GID = 1, 2, 6, 7, and 9 are shown after 5 ns for various loading configurations. Color coding is used to differentiate grains.
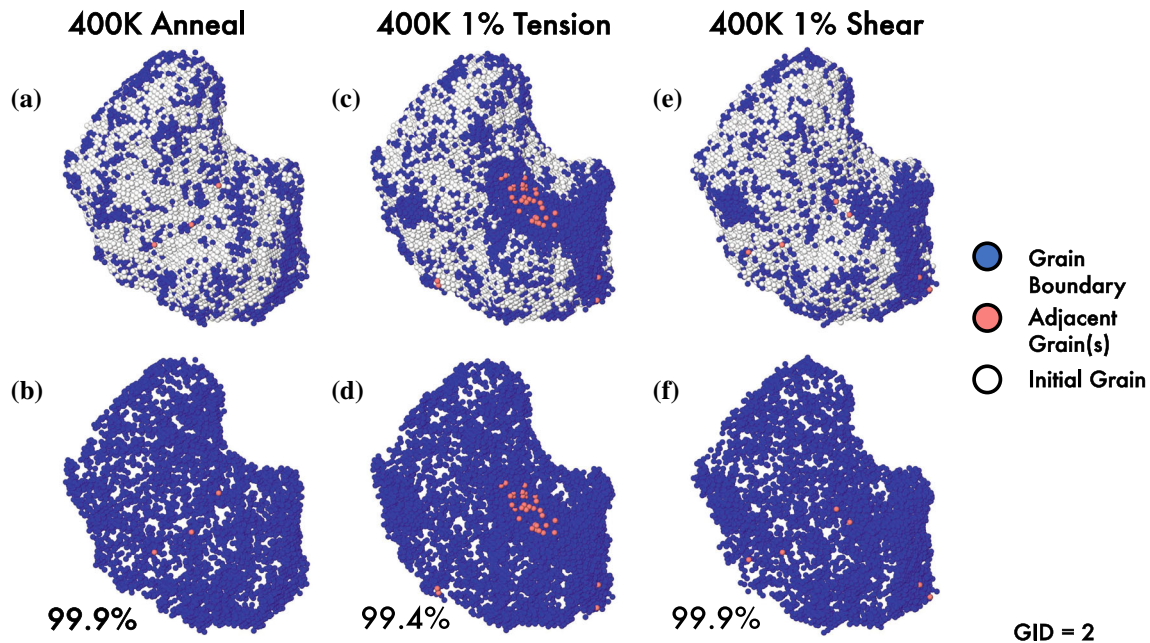
Figure 7 *Grain growth by normal grain-boundary motion for grain GID = 2 at 400 K*. Grey atoms were initial present in the grain. Blue atoms converted from grain boundary atoms into grain interior atoms during growth. And red atoms were acquired from neighboring grains and converted into grain interior atoms during growth. Final grain configuration with and without the initial core grain for **a**, **b** simple anneal at 400 K, **c**, **d** 1% tensile cyclic loading at 400 K, **e**, **f** 1% shear cyclic loading at 400 K. In all cases, over 99% of the grain growth is dominated by atoms initially in the grain boundary, grain growth mechanism is primarily driven by grain-boundary mobility and is approximately isotropic in shape. The cluster of red atoms in the 400 K tension case suggests a slight preference for growth of a specific grain boundary, but a vast majority of the growth (99.4%) occurred isotropically on all grain boundaries.

a cyclic loading. These accelerated growths remain approximately isotropic in response to the added mechanical energy provided to the nanowire during cyclic loading. Finally, the mechanically decelerated grain GID = 7 is shown for baseline anneal and 1% shear at 600 K. In this case, we note a small difference in the grain shape after 5 ns between the annealing and shear cyclic loading. However the final grain growth still remains isotropic in nature. Indeed, the only geometrical effect we can conclude is that large initial grains are stable enough to survive thermo-mechanical fluctuations and experience growth in the long term. As shown in Fig. 7, our analysis reveals that the largest grains tend to grow via normal grain-boundary motion and expansion of the volume of those grains. For instance, we show that the growth mechanism of grain GID = 2 (second largest initial grain) is dominated by atoms initially in the grain boundary, i.e., by grain-boundary motion. While the cyclic mechanical loads are shown to accelerate the overall grain growth in Fig. 5, the final grain shapes in Fig. 7 do not change, and growth remains

approximately isotropic throughout. The difference between these three cases is the varying degree of grain-boundary mobility enhancement with the applied external stimulus (thermal vs. thermo-mechanical loading).

We also observed one abnormal grain growth process in the simulations with the abrupt rotation of a smaller neighbor grain into coincidence with the parent grain. This behavior was only observed at the elevated temperature of 600 K but did not make the cutoff of the 10 largest grains. This mechanism is illustrated in Fig. 8a, b. Here, we show the abrupt grain rotation occurring between grain pair GID = 21 and GID = 192. Initially the larger grain (GID = 21) and smaller grain (GID = 192) are separated by a grain-boundary plane, and an approximate 36° of misorientation. During thermo-mechanical cycling, the smaller grain experiences a rapid rotation and alignment and merges with the larger, more stable grain. The trigger of grain rotation appears to be stochastic in nature, as abrupt growth occurs randomly within the 5 ns relaxation time of our
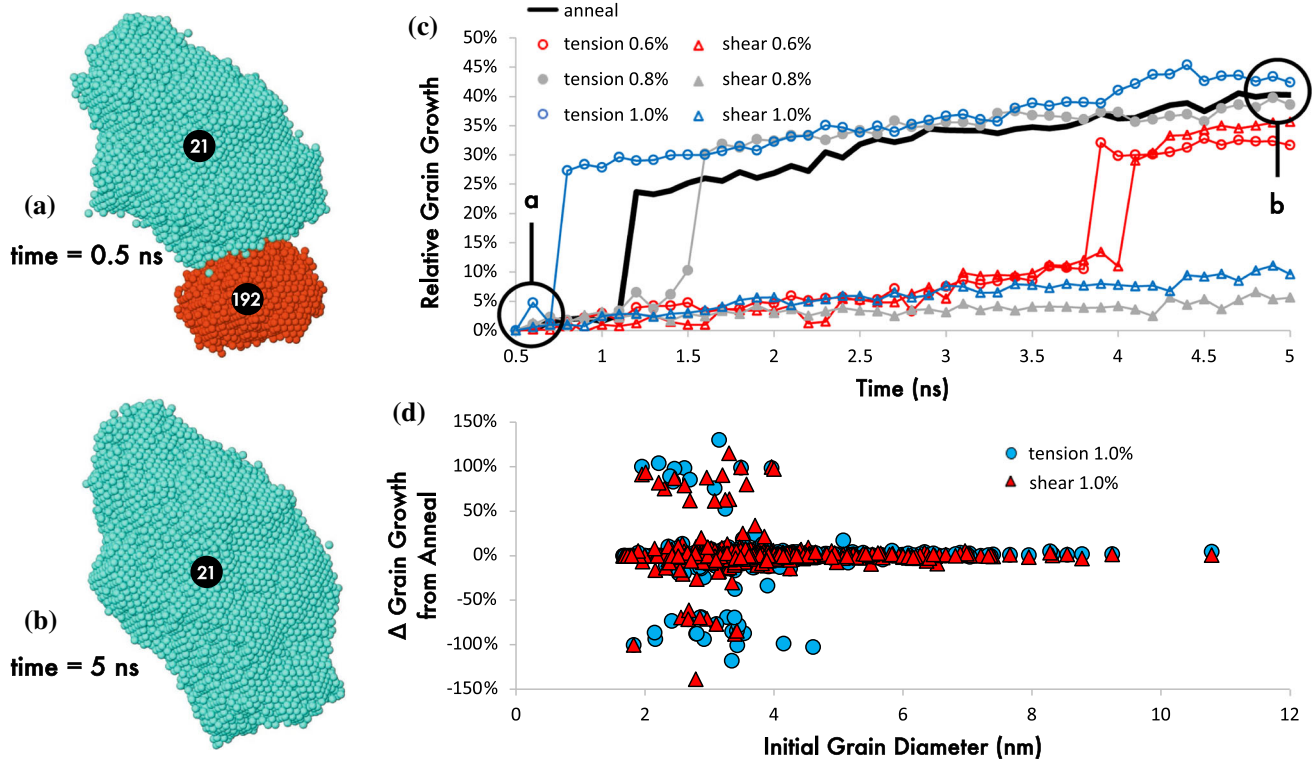
Figure 8 *Grain reorientation at 600 K.* **a** Isolated grains GID = 21 and 192. Initially small grain-boundary plane separates the two grains. **b** Abrupt reorientation and merging of grains GID = 21 and 192 at 600 K anneal. **c** Relative growth of grain GID = 21 under different mechanical loading conditions. Abrupt rotation and merging of the smaller grain appear as a sharp spike in growth. This process is completely absent at 400 K. Misorientation between GID = 21 and 192 is approximate 36°. **d** Variability in grain-growth behavior with respect to 600 K anneal for individual grains. Small grains are more sensitive to tensile and shear loads.

simulation. The process is also predominately thermally driven, as it appeared in the majority of the loading cases at 600 K. Such a mechanism may not be observed in isolation and is the result of the combination of thermal, mechanical, and grain network effects. In fact, a closer look at the relative change in growth behavior as a function of the mechanical loading mode and initial size of the grains in Fig. 8 (d) shows that smaller grains are the most impacted by the mechanical loads and therefore the most likely to experience a change in their growth mechanisms, such as grain reorientation. However, the overall, average grain growth still remains dominated by the largest grains within the microstructure.

Conclusion

In this study, we have simulated grain growth in a Pt nanowire under various thermo-mechanical, cyclic loading conditions. Examination of the grain growth of multiple grains revealed a complex set of behavior trends beyond the traditional grain-boundary driven theories. The average rate of grain growth does not scale with any definition of grain size. The addition of mechanical cyclic loading can generally accelerate grain growth; however the effects are non-uniform and vary on a grain by grain basis. The magnitude and type of mechanical loading mode (tension vs. shear) affect each grain differently. The temperature also has a complex confounding effect—low (0.6%) cyclic shear strains generally accelerate grain growth at 400 K but suppressed grain growth at 600 K. Not only are the grain-growth behaviors disparate amongst the grain population, but so are the associated atomistic growth mechanisms. We show that growth mechanisms of the largest grain remain largely dominated by normal motion of the grain boundary, while smaller grain can experience other growth mechanisms. Perhaps the most surprising result is that the grain growth at this scale appears to be largely uniform in all directions (isotropic),

seemingly independent of the character of any particular grain boundary or neighboring grain orientation. We observed abnormal grain growth in smaller grains which corresponded to an abrupt neighbor grain rotation at high temperature. This study illustrates the complexity associated with coupled thermo-mechanical grain growth at the microstructural scale and suggests a heterogeneous susceptibility to multiple competing growth processes.

Declarations

Conflict of interest The authors declare no competing interests.

References

[1] Beck PA, Sperry PR (1950) Strain induced grain boundary migration in high purity aluminum. J Appl Phys 21(2):150–152. https://doi.org/10.1063/1.1699614

[2] Li CH, Edwards EH, Washburn J, Parker ER (1953) Stress-induced movement of crystal boundaries. Acta Metall 1(2):223–229. https://doi.org/10.1016/0001-6160(53)90062-5

[3] Bainbridge DW, Choh HL, Edwards EH (1954) Recent observations on the motion of small angle dislocation boundaries. Acta Metall 2(2):322–333. https://doi.org/10.1016/0001-6160(54)90175-3

[4] Aust KT, Dunn CG (1957) Structural changes associated with strain-induced grain boundary migration in Si–Fe. JOM 9(4):472–478. https://doi.org/10.1007/BF03397902

[5] Gianola DS, Van Petegem S, Legros M, Brandstetter S, Van Swygenhoven H, Hemker KJ (2006) Stress-assisted discontinuous grain growth and its effect on the deformation behavior of nanocrystalline aluminum thin films. Acta Mater 54(8):2253–2263. https://doi.org/10.1016/j.actamat.2006.01.023

[6] Fan G, Wang Y, Fu L, Choo H, Liaw P, Ren Y, Browning N (2006) Orientation-dependent grain growth in a bulk nanocrystalline alloy during the uniaxial compressive deformation. Appl Phys Lett 88(17):171914. https://doi.org/10.1063/1.2200589

[7] Rupert TJ, Gianola DS, Gan Y, Hemker KJ (2009) Experimental observations of stress-driven grain boundary migration. Science 326(5960):1686–1690. https://doi.org/10.1126/science.1178226

[8] Sharon JA, Su PC, Prinz FB, Hemker KJ (2011) Stress-driven grain growth in nanocrystalline Pt thin films. Scr Mater 64(1):25–28. https://doi.org/10.1016/j.scriptamat.2010.08.057

[9] Liao XZ, Kilmametov AR, Valiev RZ, Gao H, Li X, Mukherjee AK, Bingert JF, Zhu YT (2006) High-pressure torsion-induced grain growth in electrodeposited nanocrystalline Ni. Appl Phys Lett 88(2):021909. https://doi.org/10.1063/1.2159088

[10] Ni S, Wang YB, Liao XZ, Alhajeri SN, Li HQ, Zhao YH, Lavernia EJ, Ringer SP, Langdon TG, Zhu YT (2011) Grain growth and dislocation density evolution in a nanocrystalline

Ni–Fe alloy induced by high-pressure torsion. Scr Mater 64(4):327–330. https://doi.org/10.1016/j.scriptamat.2010.10.027

[11] Jin M, Minor AM, Stach EA, Morris JW Jr (2004) Direct observation of deformation-induced grain growth during the nanoindentation of ultrafine-grained Al at room temperature. Acta Mater 52(18):5381–5387. https://doi.org/10.1016/j.actamat.2004.07.044

[12] Prasad M, Chokshi A (2012) Deformation-induced thermally activated grain growth in nanocrystalline nickel. Scr Mater 67(2):133–136. https://doi.org/10.1016/j.scriptamat.2012.03.041

[13] Boyce BL, Padilla HA (2011) Anomalous fatigue behavior and fatigue-induced grain growth in nanocrystalline nickel alloys. Metall Mater Trans A 42(7):1793–1804. https://doi.org/10.1007/s11661-011-0708-x

[14] Meirom RA, Alsem DH, Romasco AL, Clark T, Polcawich RG, Pulskamp JS, Dubey M, Ritchie RO, Muhlstein CL (2011) Fatigue-induced grain coarsening in nanocrystalline platinum films. Acta Mater 59(3):1141–1149. https://doi.org/10.1016/j.actamat.2010.10.047

[15] Furnish TA, Mehta A, Van Campen D, Bufford DC, Hattar K, Boyce BL (2017) The onset and evolution of fatigue-induced abnormal grain growth in nanocrystalline Ni–Fe. J Mater Sci 52(1):46–59. https://doi.org/10.1007/s10853-016-0437-z

[16] Kapp MW, Renk O, Leitner T, Ghosh P, Yang B, Pippan R (2017) Cyclically induced grain growth within shear bands investigated in UFG Ni by cyclic high pressure torsion. J Mater Res 32(23):4317–4326. https://doi.org/10.1557/jmr.2017.273

[17] Kapp MW, Kremmer T, Motz C, Yang B, Pippan R (2017) Structural instabilities during cyclic loading of ultrafine-grained copper studied with micro bending experiments. Acta Mater 125:351–358. https://doi.org/10.1016/j.actamat.2016.11.040

[18] Glushko O, Dehm G (2019) Initiation and stagnation of room temperature grain coarsening in cyclically strained gold films. Acta Mater 169:99–108. https://doi.org/10.1016/j.actamat.2019.03.004

[19] Zhao P, Chen B, Kelleher J, Yuan G, Guan B, Zhang X, Tu S (2019) High-cycle-fatigue induced continuous grain growth in ultrafine-grained titanium. Acta Mater 174:29–42. https://doi.org/10.1016/j.actamat.2019.05.038

[20] Zhang K, Weertman JR, Eastman JA (2005) Rapid stress-driven grain coarsening in nanocrystalline Cu at ambient and cryogenic temperatures. Appl Phys Lett 87(6):061921. https://doi.org/10.1063/1.2008377

[21] Sansoz F, Dupont V (2006) Grain growth behavior at absolute zero during nanocrystalline metal indentation. Appl Phys Lett 89(11):111901. https://doi.org/10.1063/1.2352725

[22] Brons JG, Padilla HA II, Thompson GB, Boyce BL (2013) Cryogenic indentation-induced grain growth in nanotwinned copper. Scr Mater 68(10):781–784. https://doi.org/10.1016/j.scriptamat.2012.12.026

[23] Frazer D, Bair JL, Homer ER, Hosemann P (2020) Cryogenic stress-driven grain growth observed via microcompression with in situ electron backscatter diffraction. JOM 72(5):2051–2056

[24] Zhang H, Mendelev MI, Srolovitz DJ (2004) Computer simulation of the elastically driven migration of a flat grain boundary. Acta Mater 52(9):2569–2576. https://doi.org/10.1016/j.actamat.2004.02.005

[25] Cahn JW, Mishin Y, Suzuki A (2006) Coupling grain boundary motion to shear deformation. Acta Mater 54(19):4953–4975. https://doi.org/10.1016/j.actamat.2006.08.004

[26] Olmsted DL, Holm EA, Foiles SM (2009) Survey of computed grain boundary properties in face-centered cubic metals-II: grain boundary mobility. Acta Mater 57(13):3704–3713. https://doi.org/10.1016/j.actamat.2009.04.015

[27] Tucker GJ, Zimmerman JA, McDowell DL (2009) Shear deformation kinematics of bicrystalline grain boundaries in atomistic simulations. Model Simul Mat Sci Eng 18(1):015002. https://doi.org/10.1088/0965-0393/18/1/015002

[28] Bhattacharyya S, Heo TW, Chang K, Chen L-Q (2011) A phase-field model of stress effect on grain boundary migration. Model Simul Mat Sci Eng 19(3):035002. https://doi.org/10.1088/0965-0393/19/3/035002

[29] Trautt ZT, Adland A, Karma A, Mishin Y (2012) Coupled motion of asymmetrical tilt grain boundaries: molecular dynamics and phase field crystal simulations. Acta Mater 60(19):6528–6546. https://doi.org/10.1016/j.actamat.2012.08.018

[30] Berbenni S, Paliwal B, Cherkaoui M (2013) A micromechanics-based model for shear-coupled grain boundary migration in bicrystals. Int J Plast 44:68–94. https://doi.org/10.1016/j.ijplas.2012.11.011

[31] Rajabzadeh A, Mompiou F, Legros M, Combe N (2013) Elementary mechanisms of shear-coupled grain boundary migration. Phys Rev Lett 110(26):265507. https://doi.org/10.1103/PhysRevLett.110.265507

[32] Wan L, Ishii A, Du J-P, Han W-Z, Mei Q, Ogata S (2017) Atomistic modeling study of a strain-free stress driven grain boundary migration mechanism. Scr Mater 134:52–56. https://doi.org/10.1016/j.scriptamat.2017.02.041

[33] Aramfard M, Deng C (2018) Mechanically enhanced grain boundary structural phase transformation in Cu. Acta Mater 146:304–313. https://doi.org/10.1016/j.actamat.2017.12.062

[34] Gao Y-J, Deng Q-Q, Liu Z-Y, Huang Z-J, Li Y-X, Luo Z-R (2020) Modes of grain growth and mechanism of dislocation reaction under applied biaxial strain: atomistic and continuum modeling. J Mater Sci Technol 49:236–250. https://doi.org/10.1016/j.jmst.2020.01.030

[35] Haslam AJ, Moldovan D, Yamakov V, Wolf D, Phillpot SR, Gleiter H (2003) Stress-enhanced grain growth in a nanocrystalline material by molecular-dynamics simulation. Acta Mater 51(7):2097–2112. https://doi.org/10.1016/S1359-6454(03)00011-9

[36] Farkas D, Frøseth A, Van Swygenhoven H (2006) Grain boundary migration during room temperature deformation of nanocrystalline Ni. Scr Mater 55(8):695–698. https://doi.org/10.1016/j.scriptamat.2006.06.032

[37] Velasco M, Van Swygenhoven H, Brandl C (2011) Coupled grain boundary motion in a nanocrystalline grain boundary network. Scr Mater 65(2):151–154. https://doi.org/10.1016/j.scriptamat.2011.03.039

[38] Schäfer J, Albe K (2012) Competing deformation mechanisms in nanocrystalline metals and alloys: coupled motion versus grain boundary sliding. Acta Mater 60(17):6076–6085. https://doi.org/10.1016/j.actamat.2012.07.044

[39] Aramfard M, Deng C (2014) Influences of triple junctions on stress-assisted grain boundary motion in nanocrystalline materials. Model Simul Mat Sci Eng 22(5):055012. https://doi.org/10.1088/0965-0393/22/5/055012

[40] Wang P, Yang X, Peng D (2016) Molecular dynamics investigation of the grain boundary migration hysteresis of nanocrystalline Ni under cyclic shear loading. Model Simul Mat Sci Eng 28(2):025006. https://doi.org/10.1088/1361-651X/aa5330

[41] Zhang Y, Tucker GJ, Trelewicz JR (2017) Stress-assisted grain growth in nanocrystalline metals: grain boundary mediated mechanisms and stabilization through alloying. Acta Mater 131:39–47. https://doi.org/10.1016/j.actamat.2017.03.060

[42] Panzarino JF, Ramos JJ, Rupert TJ (2015) Quantitative tracking of grain structure evolution in a nanocrystalline metal during cyclic loading. Model Simul Mat Sci Eng 23(2):025005. https://doi.org/10.1088/0965-0393/23/2/025005

[43] Foiles SM, Abdeljawad F, Moore A, Boyce BL (2019) Fatigue-driven acceleration of abnormal grain growth in nanocrystalline wires. Model Simul Mat Sci Eng 27(2):025008

[44] Thompson AP, Aktulga HM, Berger R, Bolintineanu DS, Brown WM, Crozier PS, in 't Veld PJ, Kohlmeyer A, Moore SG, Nguyen TD, Shan R, Stevens MJ, Tranchida J, Trott C, Plimpton SJ (2022) LAMMPS—a flexible simulation tool for particle-based materials modeling at the atomic, meso, and continuum scales. Comput Phys Commun 271:108171. https://doi.org/10.1016/j.cpc.2021.108171

[45] Stukowski A (2009) Visualization and analysis of atomistic simulation data with OVITO-the open visualization tool. Model Simul Mat Sci Eng 18(1):015012

[46] Sheng HW, Kramer MJ, Cadien A, Fujita T, Chen MW (2011) Highly optimized embedded-atom-method potentials for fourteen FCC metals. Phys Rev B 83:134118. https://doi.org/10.1103/PhysRevB.83.134118

[47] Dingreville R, Battaile CC, Brewer LN, Holm EA, Boyce BL (2010) The effect of microstructural representation on simulations of microplastic ratcheting. Int J Plast 26(5):617–633. https://doi.org/10.1016/j.ijplas.2009.09.004

[48] Gruber J, Lim H, Abdeljawad F, Foiles S, Tucker GJ (2017) Development of physically based atomistic microstructures: the effect on the mechanical response of polycrystals. Comput Mater Sci 128:29–36. https://doi.org/10.1016/j.commatsci.2016.07.011

[49] Grønbech-Jensen N (2020) Complete set of stochastic Verlet-type thermostats for correct Langevin simulations. Mol Phys 118(8):1662506. https://doi.org/10.1080/00268976.2019.1662506

[50] Panzarino JF, Rupert TJ (2014) Tracking microstructure of crystalline materials: a post-processing algorithm for atomistic simulations. JOM 66(3):417–428. https://doi.org/10.1007/s11837-013-0831-9

[51] Hoffrogge PW, Barrales-Mora LA (2017) Grain-resolved kinetics and rotation during grain growth of nanocrystalline aluminium by molecular dynamics. Comput Mater Sci 128:207–222. https://doi.org/10.1016/j.commatsci.2016.11.027

[52] Louat NP (1974) On the theory of normal grain growth. Acta Metall 22(6):721–724. https://doi.org/10.1016/0001-6160(74)90081-9

[53] Radhakrishnan B, Zacharia T (1995) Simulation of curvature-driven grain growth by using a modified Monte Carlo algorithm. Metall Mater Trans A 26(1):167–180. https://doi.org/10.1007/BF02669802